

Determination of fragmentation functions and their uncertainties

M. Hirai,^{1,*} S. Kumano,^{2,3,†} T.-H. Nagai,^{3,‡} and K. Sudoh^{2,§}

¹*Department of Physics, Tokyo Institute of Technology
Ookayama, Meguro-ku, Tokyo, 152-8550, Japan*

²*Institute of Particle and Nuclear Studies
High Energy Accelerator Research Organization (KEK)
1-1, Ooho, Tsukuba, Ibaraki, 305-0801, Japan*

³*Department of Particle and Nuclear Studies
Graduate University for Advanced Studies
1-1, Ooho, Tsukuba, Ibaraki, 305-0801, Japan*

(Dated: September 27, 2018)

Fragmentation functions and their uncertainties are determined for pion, kaon, and proton by a global χ^2 analysis of charged-hadron production data in electron-positron annihilation and by the Hessian method for error estimation. It is especially important that the uncertainties of the fragmentation functions are estimated in this analysis. The results indicate that the fragmentation functions, especially gluon and light-quark fragmentation functions, have large uncertainties at small Q^2 . There are large differences between widely-used functions by KKP (Kniehl, Kramer, and Pötter) and Kretzer; however, they are compatible with each other and also with our functions if the uncertainties are taken into account. We find that determination of the fragmentation functions is improved in next-to-leading-order (NLO) analyses for the pion and kaon in comparison with leading-order ones. Such a NLO improvement is not obvious in the proton. Since the uncertainties are large at small Q^2 , the uncertainty estimation is very important for analyzing hadron-production data at small Q^2 or p_T ($Q^2, p_T^2 \ll M_Z^2$) in lepton scattering and hadron-hadron collisions. A code is available for general users for calculating obtained fragmentation functions.

PACS numbers: 13.87.Fh, 13.66.Bc, 13.85.Ni

I. INTRODUCTION

In finding any exotic physics signatures beyond the standard model and any new hadronic systems in high-energy hadron reactions, for example at RHIC (Relativistic Heavy Ion Collider) and LHC (Large Hadron Collider), it is necessary to have accurate QCD (Quantum Chromodynamics) predictions for cross sections. The perturbative QCD is now understood in the next-to-leading-order (NLO) level for many reactions and in the next-to-next-to-leading order (NNLO) for some processes. Therefore, the crucial part is to understand non-perturbative aspects, namely parton distribution functions (PDFs) and fragmentation functions.

Fragmentation functions are used in high-energy reaction processes with hadron production. They include hadron-production processes in electron-positron annihilation, electron, muon, and neutrino scattering from proton or nucleus, proton-proton collisions, and heavy-ion collisions [1, 2]. Such reactions are becoming increasingly important in hadron physics for investigating the origin of the proton spin and quark-hadron matters in heavy-ion reactions.

The fragmentation functions are related to a nonper-

turbative aspect of QCD, so that they cannot be precisely calculated by theoretical methods at this stage. The situation is similar to the determination of the PDFs, where high-energy experimental data are used for their determination instead of theoretical calculations. There are already several studies on such analyses [3]. Widely used parametrizations were obtained by Kniehl, Kramer, and Pötter (KKP) [4] and also by Kretzer [5]. An updated version was reported recently by Albino, Kniehl, and Kramer (AKK) [4]. The fragmentation functions were determined by analyzing the hadron-production data in the e^+e^- annihilation. The analysis was done in leading order (LO) and NLO of running coupling constant α_s .

Despite the importance of the fragmentation functions, it is unfortunate that uncertainties of the fragmentation functions have not been estimated yet. The uncertainties have been investigated extensively for unpolarized PDFs [6], polarized PDFs [7], and nuclear PDFs [8]. In order to extract any information from the hadron-production processes, reliability regions of the fragmentation functions should be shown in comparison with actual data. In particular, it is known that there are large differences between the functions of KKP and Kretzer, for example between their gluon functions. An error analysis should be done for the fragmentation functions.

In this paper, we analyze the e^+e^- data for obtaining the fragmentation functions and their uncertainties in both LO and NLO. In particular, this analysis is the first attempt for showing the uncertainties of the fragmentation functions. Therefore, our works focus on

- determination of the fragmentation functions and

*E-mail: mhirai@th.phys.titech.ac.jp

†E-mail: shunzo.kumano@kek.jp

‡E-mail: tnagai@post.kek.jp

§E-mail: kazutaka.sudoh@kek.jp

their uncertainties for pion, kaon, and proton in both LO and NLO,

- roles of NLO terms on the fragmentation-function determination, namely on their uncertainties,
- comparison with other analysis results by considering the uncertainties.

The functions are defined at an initial Q^2 point in terms of a number of parameters, which are determined so as to explain the $e^+ + e^- \rightarrow h + X$ data, where $h = \pi^\pm, K^\pm$, and p/\bar{p} . The uncertainties are calculated by the Hessian method, which has been used for obtaining the PDF uncertainties in Refs. [6, 7, 8].

This paper is organized as follows. A formalism is discussed in Sec. II for hadron-production cross sections in the e^+e^- annihilation with the fragmentation functions. In Sec. III, our analysis method is described for determining the fragmentation functions. Analysis results are explained in Sec. IV. The results are summarized in Sec. V. In Appendix A, we explain how to use the obtained functions to other hadrons, π^0, K^0, \bar{K}^0, n , and \bar{n} .

II. FORMALISM

A. Hadron production in e^+e^- annihilations

The cross section for the reaction $e^+ + e^- \rightarrow h + X$ is described by two step processes [9]. The first part is to create a quark-antiquark pair by the reaction $e^+e^- \rightarrow q\bar{q}$, and higher-order corrections such as $e^+e^- \rightarrow q\bar{q}g$ are also taken into account in the NLO analysis. The second part is to create a hadron h from quark (q), antiquark (\bar{q}), or gluon (g), and this process is called fragmentation.

The fragmentation function is defined by the hadron-production cross section and the total hadronic cross section [10]:

$$F^h(z, Q^2) = \frac{1}{\sigma_{tot}} \frac{d\sigma(e^+e^- \rightarrow hX)}{dz}, \quad (1)$$

where Q^2 is the virtual photon or Z momentum squared in $e^+e^- \rightarrow \gamma, Z$ and it is given by $Q^2 = s$ with the center-of-mass energy \sqrt{s} . The variable z is defined by the energy fraction:

$$z \equiv \frac{E_h}{\sqrt{s}/2} = \frac{2E_h}{Q}, \quad (2)$$

where E_h and $\sqrt{s}/2$ are the hadron and beam energies, respectively. Namely, it indicates the hadron energy scaled to the beam energy.

The total cross section is described by the $q\bar{q}$ -pair creation processes, $e^+e^- \rightarrow \gamma \rightarrow q\bar{q}$ and $e^+e^- \rightarrow Z \rightarrow q\bar{q}$, with higher-order corrections:

$$\sigma_{tot} = \sum_q \sigma_0^q(s) \left[1 + \frac{\alpha_s(Q^2)}{\pi} \right], \quad (3)$$

where the perturbative correction is included up to the NLO. In the LO analysis, the second term is removed. The electroweak cross section for producing a $q\bar{q}$ pair is given by [11]

$$\sigma_0^q(s) = \frac{4\pi\alpha^2}{s} [e_q^2 + 2e_q c_V^e c_V^q \rho_1(s) + (c_V^{e^2} + c_A^{e^2})(c_V^{q^2} + c_A^{q^2})\rho_2(s)], \quad (4)$$

where the terms with $\rho_1(s)$ and $\rho_2(s)$ come from γ - Z interference and Z processes, and they are given by

$$\rho_1(s) = \frac{1}{4 \sin^2 \theta_W \cos^2 \theta_W} \frac{s(M_Z^2 - s)}{(M_Z^2 - s)^2 + M_Z^2 \Gamma_Z^2},$$

$$\rho_2(s) = \left(\frac{1}{4 \sin^2 \theta_W \cos^2 \theta_W} \right)^2 \frac{s^2}{(M_Z^2 - s)^2 + M_Z^2 \Gamma_Z^2}. \quad (5)$$

Here, α is the fine structure constant in Quantum Electrodynamics (QED), e_q is a quark charge, and θ_W is the weak-mixing angle. The mass and width of Z are denoted by M_Z and Γ_Z , respectively. The vector and axial-vector couplings c_V^f and c_A^f of a fermion f are expressed by the third component of the weak isospin T_f^3 and the fermion charge e_f :

$$c_V^f = T_f^3 - 2e_f \sin^2 \theta_W, \quad c_A^f = T_f^3. \quad (6)$$

Actual expressions in terms of $\sin^2 \theta_W$ are $c_V^e = -\frac{1}{2} + 2 \sin^2 \theta_W$ and $c_A^e = -\frac{1}{2}$ for the electron, $c_V^u = +\frac{1}{2} - \frac{4}{3} \sin^2 \theta_W$ and $c_A^u = +\frac{1}{2}$ for up, charm, and top quarks, and $c_V^d = -\frac{1}{2} + \frac{2}{3} \sin^2 \theta_W$ and $c_A^d = -\frac{1}{2}$ for down, strange, and bottom quarks [9].

B. Fragmentation functions and their Q^2 evolution

The fragmentation process occurs from primary quarks, antiquarks, and gluons, so that $F^h(z, Q^2)$ is expressed by the sum of their contributions [10]:

$$F^h(z, Q^2) = \sum_i C_i(z, \alpha_s) \otimes D_i^h(z, Q^2), \quad (7)$$

where $D_i^h(z, Q^2)$ is a fragmentation function of the hadron h from a parton i ($= u, d, s, \dots, g$), $C_i(z, \alpha_s)$ is a coefficient function, and the convolution integral \otimes is defined by

$$f(z) \otimes g(z) = \int_z^1 \frac{dy}{y} f(y) g\left(\frac{z}{y}\right). \quad (8)$$

The function $D_i^h(z, Q^2)$ indicates the probability to find the hadron h from a parton i with the energy fraction z . The coefficient functions are calculated in perturbative QCD, and the NLO results are listed, for example, in Refs. [4, 5, 11] for the modified minimal subtraction ($\overline{\text{MS}}$) scheme. The cross section is split into longitudinal and transverse components for the virtual γ or Z , so

that the coefficient functions are also expressed by these components.

Q^2 evolution for the fragmentation functions is calculated in the same way as the one for the PDFs by using the timelike DGLAP (Dokshitzer-Gribov-Lipatov-Altarelli-Parisi) evolution equations. For example, the flavor-singlet evolution is given by [10]

$$\frac{\partial}{\partial \ln Q^2} \begin{pmatrix} D_S^h(z, Q^2) \\ D_g^h(z, Q^2) \end{pmatrix} = \frac{\alpha_s(Q^2)}{2\pi} \begin{pmatrix} P_{qq}(z) & 2N_f P_{gq}(z) \\ P_{qg}(z) & P_{gg}(z) \end{pmatrix} \otimes \begin{pmatrix} D_S^h(z, Q^2) \\ D_g^h(z, Q^2) \end{pmatrix}, \quad (9)$$

where $D_S^h(z, Q^2)$ denotes the singlet function $D_S^h(z, Q^2) = \sum_q [D_q^h(z, Q^2) + D_{\bar{q}}^h(z, Q^2)]$, and N_f is the number of quark flavors. One should be careful that the off-diagonal elements $P_{gq}(z)$ and $P_{qg}(z)$ are interchanged in the splitting-function matrix from the PDF case. The splitting functions are the same in the LO evolution of the PDFs; however, they are different in the NLO. Explicit forms of the splitting functions are provided in Refs. [10, 12].

The evolution equations are essentially the same as the PDF case, so that the same numerical method can be applied for obtaining a solution. The equations are solved by direct integrations in the z space as explained in Ref. [13]. A slightly modified numerical approach with the Simpson's integration method is used in this analysis, and its evolution results are independently checked by using a Gauss-Legendre quadrature. Actual evolutions are calculated for the functions $D_{q^\pm}^h = D_q^h \pm D_{\bar{q}}^h$, D_S^h , and D_g^h . Then, the quark and antiquark functions are obtained by their combinations: $D_q^h = (D_{q^+}^h + D_{q^-}^h)/2$ and $D_{\bar{q}}^h = (D_{q^+}^h - D_{q^-}^h)/2$.

III. ANALYSIS METHOD

A. Parametrization

The fragmentation functions are expressed in terms of a number of parameters at the initial Q^2 ($\equiv Q_0^2$) in the same way as the PDF analysis [6, 7, 8]. Since they should vanish at $z=1$, a simple polynomial form is taken:

$$D_i^h(z, Q_0^2) = N_i^h z^{\alpha_i^h} (1-z)^{\beta_i^h}, \quad (10)$$

where N_i^h , α_i^h , and β_i^h are parameters to be determined by a χ^2 analysis of $e^+e^- \rightarrow hX$ data. This kind of polynomial form has been assumed in the parametrization studies of the fragmentation functions [4, 5]. The scale Q_0^2 is taken at mass thresholds m_c^2 and m_b^2 for charm and bottom functions, where m_c and m_b are charm- and bottom-quark masses, respectively. For the hadron h , we have pions ($\pi^+ + \pi^-$), kaons ($K^+ + K^-$), and proton/antiproton ($p + \bar{p}$).

From actual χ^2 analysis trials, we found that it is more appropriate to take the second moment M_i^h as a parameter instead of N_i^h . This is because there exists an energy sum rule

$$\sum_h M_i^h = \sum_h \int_0^1 dz z D_i^h(z, Q^2) = 1, \quad (11)$$

for the function $D_i^h(z, Q^2)$, so that M_i^h should not exceed one:

$$M_i^h < 1. \quad (12)$$

This constraint should be imposed in a global analysis. Another advantage is that the physical meaning of M_i^h is clear. It is the energy fraction for the hadron h which is created from the parton i . These parameters N_i^h and M_i^h are related with each other by

$$N_i^h = \frac{M_i^h}{B(\alpha_i^h + 2, \beta_i^h + 1)}, \quad (13)$$

where $B(\alpha_i^h + 2, \beta_i^h + 1)$ is the beta function.

A general principle of our parametrization is to use a common function for favored fragmentation functions from up and down quarks. A separate function is used for a favored one from a strange quark by considering the mass difference. Different functions are assigned for disfavored ones. Here, the favored means the fragmentation from a quark which exits in the hadron h as a constituent in the naive SU(6) quark model. The disfavored means the fragmentation from a sea quark. A flavor symmetric form is assumed for the fragmentation functions from light sea-quarks (up, down, and strange sea-quarks). Although it is known that light sea-quark distributions are not flavor symmetric in the unpolarized PDFs [14], there is no data to distinguish among the fragmentation functions from different light sea-quarks.

The actual parametrization forms are shown for the pion, kaon, and proton in the following.

(1) Pion (π^+)

Considering the constituent quark composition $\pi^+(u\bar{d})$, we take the same favored fragmentation functions for π^+ from u and \bar{d} quarks:

$$D_u^{\pi^+}(z, Q_0^2) = D_{\bar{d}}^{\pi^+}(z, Q_0^2) = N_u^{\pi^+} z^{\alpha_u^{\pi^+}} (1-z)^{\beta_u^{\pi^+}}. \quad (14)$$

The pion productions from \bar{u} , d , s , and \bar{s} are disfavored processes, and they are considered the same at the initial scale:

$$\begin{aligned} D_{\bar{u}}^{\pi^+}(z, Q_0^2) &= D_d^{\pi^+}(z, Q_0^2) \\ &= D_s^{\pi^+}(z, Q_0^2) = D_{\bar{s}}^{\pi^+}(z, Q_0^2) \\ &= N_{\bar{u}}^{\pi^+} z^{\alpha_{\bar{u}}^{\pi^+}} (1-z)^{\beta_{\bar{u}}^{\pi^+}}. \end{aligned} \quad (15)$$

In addition, a fragmentation function from gluon is given by

$$D_g^{\pi^+}(z, Q_0^2) = N_g^{\pi^+} z^{\alpha_g^{\pi^+}} (1-z)^{\beta_g^{\pi^+}}. \quad (16)$$

These functions are provided at the initial scale Q_0^2 with the parameters.

Different functions are assigned for productions from heavy quarks because of mass differences:

$$D_c^{\pi^+}(z, m_c^2) = D_{\bar{c}}^{\pi^+}(z, m_c^2) = N_c^{\pi^+} z^{\alpha_c^{\pi^+}} (1-z)^{\beta_c^{\pi^+}}, \quad (17)$$

$$D_b^{\pi^+}(z, m_b^2) = D_{\bar{b}}^{\pi^+}(z, m_b^2) = N_b^{\pi^+} z^{\alpha_b^{\pi^+}} (1-z)^{\beta_b^{\pi^+}}. \quad (18)$$

Thresholds for heavy quarks are $Q^2 = m_c^2$ and m_b^2 in calculating Q^2 evolutions and the running coupling constant $\alpha_s(Q^2)$. However, the thresholds for the cross section are taken $Q^2 = 4m_c^2$ and $4m_b^2$ [4, 5].

At different Q^2 ($\neq Q_0^2$), one should note that some equal relations do not hold in the NLO because of a $q \rightarrow \bar{q}$ or $\bar{q} \rightarrow q$ splitting [14]:

$$D_u^{\pi^+}(z, Q^2) = D_d^{\pi^+}(z, Q^2) \neq D_s^{\pi^+}(z, Q^2), \quad (19)$$

although $D_u^{\pi^+}(z, Q^2) = D_d^{\pi^+}(z, Q^2)$, $D_s^{\pi^+}(z, Q^2) = D_{\bar{s}}^{\pi^+}(z, Q^2)$, $D_c^{\pi^+}(z, Q^2) = D_{\bar{c}}^{\pi^+}(z, Q^2)$, and $D_b^{\pi^+}(z, Q^2) = D_{\bar{b}}^{\pi^+}(z, Q^2)$ are still valid.

(2) Kaon (K^+)

Parameters are assigned to K^+ fragmentation functions in the same way by considering the constituent quark composition $K^+(u\bar{s})$. The only difference is that the anti-strange function is taken in a different form from the up-quark one:

$$D_u^{K^+}(z, Q_0^2) = N_u^{K^+} z^{\alpha_u^{K^+}} (1-z)^{\beta_u^{K^+}}, \quad (20)$$

$$D_{\bar{s}}^{K^+}(z, Q_0^2) = N_{\bar{s}}^{K^+} z^{\alpha_{\bar{s}}^{K^+}} (1-z)^{\beta_{\bar{s}}^{K^+}}, \quad (21)$$

$$D_u^{K^+}(z, Q_0^2) = D_d^{K^+}(z, Q_0^2) = D_{\bar{d}}^{K^+}(z, Q_0^2) \\ = D_s^{K^+}(z, Q_0^2) = N_{\bar{u}}^{K^+} z^{\alpha_{\bar{u}}^{K^+}} (1-z)^{\beta_{\bar{u}}^{K^+}}, \quad (22)$$

$$D_c^{K^+}(z, m_c^2) = D_{\bar{c}}^{K^+}(z, m_c^2) = N_c^{K^+} z^{\alpha_c^{K^+}} (1-z)^{\beta_c^{K^+}}, \quad (23)$$

$$D_b^{K^+}(z, m_b^2) = D_{\bar{b}}^{K^+}(z, m_b^2) = N_b^{K^+} z^{\alpha_b^{K^+}} (1-z)^{\beta_b^{K^+}}, \quad (24)$$

$$D_g^{K^+}(z, Q_0^2) = N_g^{K^+} z^{\alpha_g^{K^+}} (1-z)^{\beta_g^{K^+}}. \quad (25)$$

At general Q^2 ($\neq Q_0^2$), there are differences in the NLO as explained in the pion case:

$$D_u^{K^+}(z, Q^2) \neq D_d^{K^+}(z, Q^2) \neq D_s^{K^+}(z, Q^2). \quad (26)$$

The relations $D_d^{K^+}(z, Q^2) = D_{\bar{d}}^{K^+}(z, Q^2)$, $D_c^{K^+}(z, Q^2) = D_{\bar{c}}^{K^+}(z, Q^2)$, and $D_b^{K^+}(z, Q^2) = D_{\bar{b}}^{K^+}(z, Q^2)$ are still valid in the Q^2 evolution.

(3) Proton (p)

Proton fragmentation functions are also parametrized in the same way by considering the constituent quark composition $p(uud)$:

$$D_u^p(z, Q_0^2) = 2 D_d^p(z, Q_0^2) = N_u^p z^{\alpha_u^p} (1-z)^{\beta_u^p}, \quad (27)$$

$$D_{\bar{u}}^p(z, Q_0^2) = D_{\bar{d}}^p(z, Q_0^2) = D_s^p(z, Q_0^2) \\ = D_{\bar{s}}^p(z, Q_0^2) = N_{\bar{u}}^p z^{\alpha_{\bar{u}}^p} (1-z)^{\beta_{\bar{u}}^p}, \quad (28)$$

$$D_c^p(z, m_c^2) = D_{\bar{c}}^p(z, m_c^2) = N_c^p z^{\alpha_c^p} (1-z)^{\beta_c^p}, \quad (29)$$

$$D_b^p(z, m_b^2) = D_{\bar{b}}^p(z, m_b^2) = N_b^p z^{\alpha_b^p} (1-z)^{\beta_b^p}, \quad (30)$$

$$D_g^p(z, Q_0^2) = N_g^p z^{\alpha_g^p} (1-z)^{\beta_g^p}. \quad (31)$$

The major difference from the mesons is the factor of two in $D_u^p(z, Q_0^2) = 2 D_d^p(z, Q_0^2)$ which is suggested simply by considering valence-quark structure with a flavor symmetry [4]. In order to produce a baryon from a quark, two $q\bar{q}$ pairs need to be created. If the initial quark is up quark, two creation process, $(u\bar{u})(d\bar{d})$ and $(d\bar{d})(u\bar{u})$, should contribute to the proton formation, whereas only the $(u\bar{u})(u\bar{u})$ process contributes if the down quark is in the initial state. It leads to the factor of two although it is a naive counting estimate. This factor is also the same in a spectator di-quark model in the flavor symmetric case [15].

At different Q^2 , one should be careful about the following inequalities in the NLO:

$$D_u^p(z, Q^2) \neq 2 D_d^p(z, Q^2), \quad (32)$$

$$D_{\bar{u}}^p(z, Q^2) \neq D_{\bar{d}}^p(z, Q^2) \neq D_s^p(z, Q^2). \quad (33)$$

The equalities for strange, charm, and bottom quarks, $D_s^p(z, Q^2) = D_{\bar{s}}^p(z, Q^2)$, $D_c^p(z, Q^2) = D_{\bar{c}}^p(z, Q^2)$, and $D_b^p(z, Q^2) = D_{\bar{b}}^p(z, Q^2)$, are not changed by the Q^2 evolution.

(4) π^- , K^- , and \bar{p}

In the constituent quark model, π^- , K^- , and \bar{p} are expressed $\pi^-(\bar{u}d)$, $K^-(\bar{u}s)$, and $\bar{p}(\bar{u}\bar{u}\bar{d})$. Using the charge symmetry, we relate the fragmentation functions of π^- to the ones of π^+ :

$$D_q^{\pi^-, K^-, \bar{p}}(z, Q^2) = D_{\bar{q}}^{\pi^+, K^+, p}(z, Q^2). \quad (34)$$

The gluonic functions are the same:

$$D_g^{\pi^-, K^-, \bar{p}}(z, Q^2) = D_g^{\pi^+, K^+, p}(z, Q^2). \quad (35)$$

The functions for π^0 , K^0 , \bar{K}^0 , n , and \bar{n} are also obtained by using the charge symmetry, and it is explained in Appendix A.

After all, the following parameters are used for the pion

kaon, and proton in our global analysis:

$$\begin{aligned}
\text{pion: } & \alpha_u^{\pi^+}, \beta_u^{\pi^+}, M_u^{\pi^+}, \alpha_{\bar{u}}^{\pi^+}, \beta_{\bar{u}}^{\pi^+}, M_{\bar{u}}^{\pi^+}, \\
& \alpha_c^{\pi^+}, \beta_c^{\pi^+}, M_c^{\pi^+}, \alpha_b^{\pi^+}, \beta_b^{\pi^+}, M_b^{\pi^+}, \alpha_g^{\pi^+}, \beta_g^{\pi^+}, M_g^{\pi^+}, \\
\text{kaon: } & \alpha_u^{K^+}, \beta_u^{K^+}, M_u^{K^+}, \alpha_{\bar{s}}^{K^+}, \beta_{\bar{s}}^{K^+}, M_{\bar{s}}^{K^+}, \alpha_{\bar{u}}^{K^+}, \beta_{\bar{u}}^{K^+}, M_{\bar{u}}^{K^+}, \\
& \alpha_c^{K^+}, \beta_c^{K^+}, M_c^{K^+}, \alpha_b^{K^+}, \beta_b^{K^+}, M_b^{K^+}, \alpha_g^{K^+}, \beta_g^{K^+}, M_g^{K^+}, \\
\text{proton: } & \alpha_u^p, \beta_u^p, M_u^p, \alpha_{\bar{u}}^p, \beta_{\bar{u}}^p, M_{\bar{u}}^p, \\
& \alpha_c^p, \beta_c^p, M_c^p, \alpha_b^p, \beta_b^p, M_b^p, \alpha_g^p, \beta_g^p, M_g^p.
\end{aligned}$$

B. Experimental data

The fragmentation functions are determined by the charged-hadron production data of $e^+ + e^- \rightarrow h^\pm + X$. Used data are those from the measurements of TASSO [16, 17, 18], TPC [19], HRS [20], TOPAZ [21], SLD [22], ALEPH [23], OPAL [24], and DELPHI [25, 26]. There are data from MARK-II [27] and JADE [28] collaborations; however, they are not used in our analysis because of the kinematical condition $z > 0.1$, which is explained in the following. References, center-of-mass (c.m.) energies, and numbers of the data are listed for used data sets in Tables I, II, and III [29]. The ALEPH, DELPHI, and OPAL data are taken at CERN (European Organization for Nuclear Research), TASSO at DESY (German Electron Synchrotron), TOPAZ at KEK (High Energy Accelerator Research Organization), and HRS, SLD, and TPC at SLAC (Stanford Linear Accelerator Center). In the DELPHI and SLD measurements, the light-quark and heavy-quark events are separated.

Since the perturbative QCD is applied in the Q^2 evolution calculations, the data with $Q^2 > 1 \text{ GeV}^2$ are used in our analysis. Furthermore, small- z data are excluded because of soft-gluon emission. The minimum z value is $z_{min} = 0.1$ for the data at $\sqrt{s} < M_Z$ and $z_{min} = 0.05$ for the data at $\sqrt{s} = M_Z$. Resummation effects of soft-gluon logarithms need to be clarified in order to include the small- z data into the analysis [30]. We do not include three-jet and unidentified-hadron data [4, 31]. There are ambiguities for extracting the gluon fragmentation function from three-jet cross sections [5]. In order to describe the unidentified-hadron cross sections, all the relevant hadrons need to be included in the analysis, whereas only the pions, kaons, proton, and anti-proton are taken into account in our analysis.

The kinematical range is shown in Fig. 1 by the variables z and Q ($\equiv \sqrt{Q^2} = \sqrt{s}$) for the pion data. Here, the data are also shown in the small z region ($z < 0.1$ or $z < 0.05$), where they are not included in the actual analysis. The range of Q is wide from the low-energy TASSO data to high-energy SLD, ALEPH, OPAL, and DELPHI data at $Q = M_Z$. Many data are collected in the small- z region ($z < 0.4$), whereas the large- z data are scarce because cross sections are very small.

TABLE I: Experiments, references, center-of-mass energies, and numbers of data points are listed for used data sets of $e^+ + e^- \rightarrow \pi^\pm + X$ [29].

experiment	ref.	\sqrt{s}	# of data
TASSO	[16, 17, 18]	12,14,22,30,34,44	29
TPC	[19]	29	18
HRS	[20]	29	2
TOPAZ	[21]	58	4
SLD	[22]	91.28	29
SLD (u,d,s quark)	[22]	91.28	29
SLD (c quark)	[22]	91.28	29
SLD (b quark)	[22]	91.28	29
ALEPH	[23]	91.2	22
OPAL	[24]	91.2	22
DELPHI	[25]	91.2	17
DELPHI (u,d,s quark)	[25]	91.2	17
DELPHI (b quark)	[25]	91.2	17
total			264

TABLE II: Experimental information is listed for the used data of $e^+ + e^- \rightarrow K^\pm + X$ [29].

experiment	ref.	\sqrt{s}	# of data
TASSO	[16, 17, 18]	12,14,22,30,34	18
TPC	[19]	29	17
HRS	[20]	29	3
TOPAZ	[21]	58	3
SLD	[22]	91.28	29
SLD (u,d,s quark)	[22]	91.28	29
SLD (c quark)	[22]	91.28	29
SLD (b quark)	[22]	91.28	28
ALEPH	[23]	91.2	18
OPAL	[24]	91.2	10
DELPHI	[25, 26]	91.2	27
DELPHI (u,d,s quark)	[25]	91.2	17
DELPHI (b quark)	[25]	91.2	17
total			245

TABLE III: Experimental information is listed for the used data of $e^+ + e^- \rightarrow p/\bar{p} + X$ [29].

experiment	ref.	\sqrt{s}	# of data
TASSO	[16, 17, 18]	12,14,22,30,34	24
TPC	[19]	29	17
HRS	[20]	29	4
TOPAZ	[21]	58	3
SLD	[22]	91.28	30
SLD (u,d,s quark)	[22]	91.28	30
SLD (c quark)	[22]	91.28	30
SLD (b quark)	[22]	91.28	26
ALEPH	[23]	91.2	18
OPAL	[24]	91.2	10
DELPHI	[25, 26]	91.2	23
DELPHI (u,d,s quark)	[25]	91.2	17
DELPHI (b quark)	[25]	91.2	17
total			249

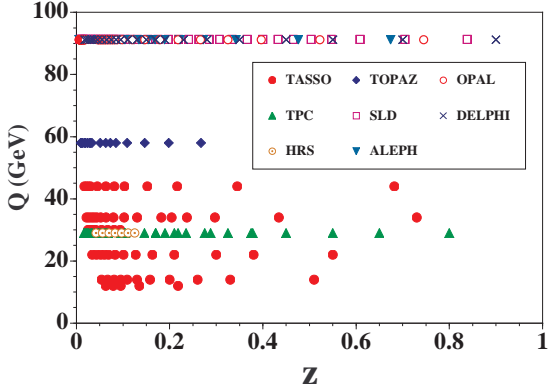


FIG. 1: (Color online) Kinematical range is shown by z and $Q(=\sqrt{s})$ values for the pion data.

C. χ^2 analysis

The total χ^2 is calculated in comparison with the data for the fragmentation function $F^h(z, Q^2)$ of the hadron h in Eq. (1). The scale Q^2 is equal to the c.m. energy squared s in Tables I, II, and III. The initial scale, where the fragmentation functions for up, down, and strange quarks are defined, is taken $Q_0^2=1$ GeV². Since the e^+e^- data are measured at large Q^2 as shown in the tables, we could have taken a larger Q_0^2 in the range where perturbative QCD can be applied undoubtedly without worrying about higher-twist and higher-order corrections. However, the fragmentation functions are practically used also in a relatively small Q^2 region, for example, in hadron-production process in deep inelastic lepton scattering [1] and proton-proton collisions [2]. For applications of obtained functions to such processes, it is better to supply a code for calculating the functions even at small Q^2 (~ 1 GeV²). Considering this situation, we decided to take $Q_0^2=1$ GeV². The heavy-quark functions are defined at the mass thresholds. The quark masses are $m_c=1.43$ GeV and $m_b=4.3$ GeV as given in Ref. [32].

The theoretical functions should be obtained at the same experimental Q^2 points for calculating χ^2 . The Q^2 evolution is calculated by the timelike DGLAP equations as explained in Sec. II B. Then, the evolved functions are convoluted with the coefficient functions in Eq. (7). These calculations depend on the choice of the scale parameter Λ . It is taken $\Lambda_{LO}^{(4)}=0.220$ GeV or $\Lambda_{NLO}^{(4)}=0.323$ GeV for four flavors [32]. The $\overline{\text{MS}}$ scheme is used in the NLO. Below the charm threshold and above the bottom one, these values are converted to corresponding ones for three and five flavors so that the coupling constant α_s is continuous at the thresholds.

The total χ^2 is then calculated by

$$\chi^2 = \sum_j \frac{(F_j^{data} - F_j^{theo})^2}{(\sigma_j^{data})^2}, \quad (36)$$

where F_j^{data} and F_j^{theo} are experimental and theoretical values of $F^h(z, Q^2)$, respectively, at the same exper-

imental Q^2 point. The experimental errors are calculated from systematic and statistical errors by $(\sigma_j^{data})^2 = (\sigma_j^{sys})^2 + (\sigma_j^{stat})^2$. The assigned parameters are determined so as to obtain the minimum χ^2 . The optimization of the functions is done by the CERN subroutine MINUIT [33].

D. Uncertainties of fragmentation functions

Uncertainties of the PDFs were estimated in Refs. [6, 7, 8]. Two methods have been developed: the Hessian and Lagrange-multiplier methods. Although technical details are described in these references, outline of the Hessian method is explained because it is used in our analysis and uncertainties have not been investigated in the fragmentations functions.

The parameters are denoted ξ_i ($i=1, 2, \dots, N$), where N is the number of the parameters. We expand χ^2 around the minimum χ^2 point $\hat{\xi}$:

$$\Delta\chi^2(\xi) = \chi^2(\hat{\xi} + \delta\xi) - \chi^2(\hat{\xi}) = \sum_{i,j} H_{ij} \delta\xi_i \delta\xi_j, \quad (37)$$

where only the leading quadratic term is kept, and the Hessian H_{ij} is the second derivative matrix. The confidence region is given in the parameter space by supplying a value of $\Delta\chi^2$. It is known that the confidence level is 68% for $\Delta\chi^2=1$ if the number of the parameters is one ($N=1$). The $\Delta\chi^2$ value needs to be changed in a general case of $N \neq 1$. Assuming correspondence between the confidence level of a normal distribution in multi-parameter space and the one of a χ^2 distribution with N degree of freedom, we have the confidence level P :

$$P = \int_0^{\Delta\chi^2} \frac{1}{2 \Gamma(N/2)} \left(\frac{S}{2}\right)^{\frac{N}{2}-1} \exp\left(-\frac{S}{2}\right) dS, \quad (38)$$

where $\Gamma(N/2)$ is the Gamma function. The value of $\Delta\chi^2$ is taken so that the confidence level becomes the one- σ -error range, namely $P = 0.6826$ [7, 8]. The details of this $\Delta\chi^2$ choice are explained in Ref. [34]. The $\Delta\chi^2$ value is numerically calculated by using Eq. (38). For example, $\Delta\chi^2 = 15.94$ is obtained for $N = 14$. The Hessian matrix is obtained by running the subroutine MINUIT. From this Hessian, $\Delta\chi^2$, and derivatives of the fragmentation functions with respect to the parameters, the uncertainties are calculated by

$$[\delta D_i^h(z)]^2 = \Delta\chi^2 \sum_{j,k} \left(\frac{\partial D_i^h(z, \xi)}{\partial \xi_j}\right)_{\hat{\xi}} H_{jk}^{-1} \left(\frac{\partial D_i^h(z, \xi)}{\partial \xi_k}\right)_{\hat{\xi}}. \quad (39)$$

IV. RESULTS

Analysis results are explained. In Sec. IV A, optimized parameters are shown, and χ^2 contributions from data sets are listed. Then, fit results are compared with experimental data. In Sec. IV B, the obtained fragmentation functions and their uncertainties are shown. They are compared with other parametrization results in Sec. IV C.

A. Comparison with experimental data

Obtained parameters in the LO and NLO are listed in Tables IV, V, and VI for the pion, kaon, and proton, respectively. In these analyses, it was very difficult to determine the gluon functions, so that we decided to fix some parameters. In trial analyses, we found that the gluon function for the pion ($zD_g^{\pi^+}$) tends to be peaked at $z \sim 0.2$. The parameter β_g controls its functional behavior at large z . Since the gluon function becomes very small at large z , the value of β_g does not affect the χ^2 value to a significant amount if the function is peaked at small z . Therefore, the parameter β_g is fixed as $\beta_g=8$ in the pion analyses. If this value is taken much more than eight, the energy sum rule in Eq. (11) is badly violated in the gluon part. If it much less than eight, it is violated in the up-quark part. The value $\beta_g=8$ is chosen to compromise these two issues. In the analysis of Kretzer [5], one of the gluon parameters is also fixed because the second moment is equal to the average of the moments of up- and down-quark fragmentation functions.

In the kaon analyses, the gluon function tends to be peaked at large z . Therefore, α_g becomes the parameter which does not affect the total χ^2 instead of β_g . It is chosen $\alpha_g = 5$ so that the moments for gluon and up quark do not become too large to affect the sum rule to a significant extent.

It was also very difficult to determine the gluon distribution for the proton. It indicates that the data are not sensitive to the gluon function at this stage even in the NLO analysis. Therefore, the moment of the gluon function is fixed at the average of the moments for the favored and disfavored functions [5]: $M_g = [(M_u + M_d)/2 + M_{\bar{u}}]/2$. Furthermore, the function tends to be peaked at large z , so that the parameter α_g is fixed at $\alpha_g = 5$ in the same way as the kaon case. The average of the moments is motivated by the following consideration. The process for producing a proton from an initial up or down quark should contain two quark-pair productions ($u\bar{u}$ and $d\bar{d}$ pairs or two $u\bar{u}$ pairs), so that it is proportional to g^4 with the strong coupling constant g . In the same way, the process from an initial \bar{u} quark is proportional to g^6 , and the one from an initial gluon is to g^5 . Therefore, the gluon moment is, roughly speaking, given by the average of favored (u and d) and disfavored (\bar{u}) moments. Such averages are also taken in Ref. [5].

TABLE IV: Parameters determined for the pion.

function	M	α	β
(LO)			
$D_u^{\pi^+}$	0.546 ± 0.085	-1.100 ± 0.183	1.282 ± 0.140
$D_{\bar{u}}^{\pi^+}$	0.250 ± 0.068	-0.500 ± 0.301	5.197 ± 0.576
$D_c^{\pi^+}$	0.305 ± 0.046	-1.007 ± 0.123	3.918 ± 0.236
$D_b^{\pi^+}$	0.302 ± 0.023	-1.176 ± 0.045	5.805 ± 0.188
$D_g^{\pi^+}$	0.115 ± 0.111	1.405 ± 0.897	8.0 (fixed)
(NLO)			
$D_u^{\pi^+}$	0.401 ± 0.052	-0.963 ± 0.177	1.370 ± 0.144
$D_{\bar{u}}^{\pi^+}$	0.094 ± 0.029	0.718 ± 0.466	6.266 ± 0.808
$D_c^{\pi^+}$	0.178 ± 0.018	-0.845 ± 0.108	3.868 ± 0.323
$D_b^{\pi^+}$	0.236 ± 0.009	-1.219 ± 0.042	5.668 ± 0.219
$D_g^{\pi^+}$	0.238 ± 0.029	1.943 ± 0.399	8.0 (fixed)

TABLE V: Parameters determined for the kaon

function	M	α	β
(LO)			
$D_u^{K^+}$	0.0922 ± 0.0419	0.588 ± 1.605	1.632 ± 0.812
$D_s^{K^+}$	0.1651 ± 0.0962	2.190 ± 2.871	2.829 ± 1.143
$D_{\bar{u}}^{K^+}$	0.0638 ± 0.0363	0.565 ± 0.460	7.093 ± 3.383
$D_c^{K^+}$	0.0919 ± 0.0055	0.230 ± 0.157	4.549 ± 0.388
$D_b^{K^+}$	0.0696 ± 0.0027	0.017 ± 0.110	8.808 ± 0.534
$D_g^{K^+}$	0.0319 ± 0.0147	5.0 (fixed)	0.247 ± 0.162
(NLO)			
$D_u^{K^+}$	0.0740 ± 0.0268	-0.630 ± 0.629	1.310 ± 0.772
$D_s^{K^+}$	0.0878 ± 0.0506	2.000 ± 2.913	2.800 ± 1.313
$D_{\bar{u}}^{K^+}$	0.0255 ± 0.0173	1.012 ± 0.939	8.000 ± 3.715
$D_c^{K^+}$	0.0583 ± 0.0052	0.527 ± 0.228	5.866 ± 0.636
$D_b^{K^+}$	0.0522 ± 0.0024	0.247 ± 0.126	11.212 ± 0.721
$D_g^{K^+}$	0.0705 ± 0.0099	5.0 (fixed)	0.810 ± 0.239

TABLE VI: Parameters determined for the proton.

function	M	α	β
(LO)			
D_u^p	0.0839 ± 0.0125	-0.814 ± 0.200	1.628 ± 0.324
$D_{\bar{u}}^p$	0.0158 ± 0.0058	0.866 ± 0.677	5.078 ± 1.400
D_c^p	0.0241 ± 0.0015	0.683 ± 0.359	7.375 ± 1.250
D_b^p	0.0180 ± 0.0006	0.071 ± 0.178	8.802 ± 0.839
D_g^p	$\frac{(M_u + M_d)/2 + M_{\bar{u}}}{2}$	5.0 (fixed)	2.927 ± 1.117
(NLO)			
D_u^p	0.0732 ± 0.0113	-1.022 ± 0.219	1.434 ± 0.268
$D_{\bar{u}}^p$	0.0084 ± 0.0057	1.779 ± 1.422	4.763 ± 1.882
D_c^p	0.0184 ± 0.0017	0.407 ± 0.373	6.784 ± 1.555
D_b^p	0.0155 ± 0.0007	-0.203 ± 0.165	8.209 ± 0.950
D_g^p	$\frac{(M_u + M_d)/2 + M_{\bar{u}}}{2}$	5.0 (fixed)	4.900 ± 2.046

TABLE VII: Each χ^2 contribution in the pion analysis.

experiment	# of data	χ^2 (LO)	χ^2 (NLO)
TASSO	29	52.1	51.9
TPC	18	33.5	27.3
HRS	2	1.1	2.0
TOPAZ	4	2.6	2.6
SLD (all)	29	11.3	10.6
SLD (u,d,s)	29	46.0	36.4
SLD (c)	29	24.4	26.1
SLD (b)	29	71.2	66.4
ALEPH	22	22.8	24.0
OPAL	22	45.4	45.8
DELPHI (all)	17	48.3	48.6
DELPHI (u,d,s)	17	29.6	31.1
DELPHI (b)	17	64.9	60.8
total	264	453.2	433.5
(/d.o.f.)		(1.81)	(1.73)

 TABLE VIII: Each χ^2 contribution in the kaon analysis.

experiment	# of data	χ^2 (LO)	χ^2 (NLO)
TASSO	18	26.8	25.0
TPC	17	15.2	15.2
HRS	3	0.6	0.4
TOPAZ	3	0.5	0.8
SLD (all)	29	14.9	12.3
SLD (u,d,s)	29	58.8	57.2
SLD (c)	29	33.6	32.4
SLD (b)	28	127.7	88.7
ALEPH	18	10.3	12.8
OPAL	10	10.6	11.5
DELPHI (all)	27	14.8	15.2
DELPHI (u,d,s)	17	22.5	22.1
DELPHI (b)	17	11.7	11.7
total	245	348.2	305.1
(/d.o.f.)		(1.53)	(1.34)

 TABLE IX: Each χ^2 contribution in the proton/anti-proton analysis.

experiment	# of data	χ^2 (LO)	χ^2 (NLO)
TASSO	24	34.9	33.6
TPC	17	22.6	23.5
HRS	4	19.5	16.3
TOPAZ	3	3.6	3.2
SLD (all)	30	13.0	12.6
SLD (u,d,s)	30	62.9	56.6
SLD (c)	30	46.3	47.1
SLD (b)	26	36.3	37.9
ALEPH	18	15.7	15.8
OPAL	10	112.1	110.6
DELPHI (all)	23	5.6	6.4
DELPHI (u,d,s)	17	2.1	2.4
DELPHI (b)	17	16.5	17.1
total	249	391.2	383.2
(/d.o.f.)		(1.66)	(1.62)

The difficulty in determining the gluon function is reflected in large errors of the gluon parameters as shown in Tables IV, V, and VI. The light-quark (u, \bar{u}, \bar{s}) functions also have large errors which are as large as the gluon ones. The values of the second moments M_i^h indicate that a large fraction for the final hadrons comes from the pions. Kaon and proton contributions are rather small. The moments also indicate that the favored functions are generally larger than the disfavored ones as expected. Adding these moments, we find that the total moments are generally within the energy sum rule in Eq. (11). However, the sums slightly exceed one for the gluon and up quark. Considering the errors in the moments, we did not strictly impose the sum-rule condition. We found a general tendency that the moment errors for the pion become smaller in the NLO in comparison with the LO, whereas the NLO errors are as large as the LO ones for the kaon and proton. Although many used data are taken at large Q^2 as shown in Fig. 1, the pion data are sensitive to the NLO corrections in the Q^2 evolution and coefficient functions.

Each χ^2 contribution is listed in Tables VII, VIII, and IX for the pion, kaon, and proton/anti-proton, respectively. The χ^2 values indicate that the pion data of HRS, TOPAZ, SLD (all; $u,d,s; c$), and ALEPH are explained by our parametrization, whereas TASSO, TPC, SLD (b), OPAL, and DELPHI (all; $u,d,s; b$) data are not so well reproduced. In the kaon analysis, the situation is slightly different. The data of TPC, HRS, TOPAZ, SLD (all; c), ALEPH, OPAL, and DELPHI (all; $u,d,s; b$) are now well explained by our fits, whereas the data of TASSO and SLD ($u,d,s; b$) deviate. In the proton analysis, the data of TPC, TOPAZ, SLD(all), ALEPH, and DELPHI (all; $u,d,s; b$) are well explained; however, the data of TASSO, HRS, SLD ($u,d,s; c; b$), and OPAL are not reproduced. Some data sets deviate significantly from our parametrization, namely from other data sets. For example, the χ^2 value is more than hundred for ten data points in the OPAL proton data.

In Fig. 2, our NLO parametrization results are compared with the data at $Q = M_Z$ without separation on initial partons by the ALEPH, DELPHI, OPAL, and SLD collaborations. The figure shows the comparison with the pion data for $F^{\pi^\pm}(z, Q^2)$ in Eq. (1). Here, π^\pm indicates charged pions: $\pi^\pm = \pi^+ + \pi^-$. The one- σ range of the uncertainty band is shown by the shaded area. The theoretical curve and its uncertainty are calculated at $Q = M_Z$. Most of the data are explained by the parametrization and they are within the uncertainty band. However, some DELPHI data are outside the band, which leads to the large χ^2 contribution in Table VII.

Next, the NLO results are compared with each data set for the pion in Figs. 3 and 4, where the data for the initial-quark separation are also shown. The figure indicates the rational difference between the data and the theoretical parametrization: $[F^{\pi^\pm}(\text{data}) - F^{\pi^\pm}(\text{theory})]/F^{\pi^\pm}(\text{theory})$ at the same Q^2 point with the data. Most of the data are compatible with the NLO

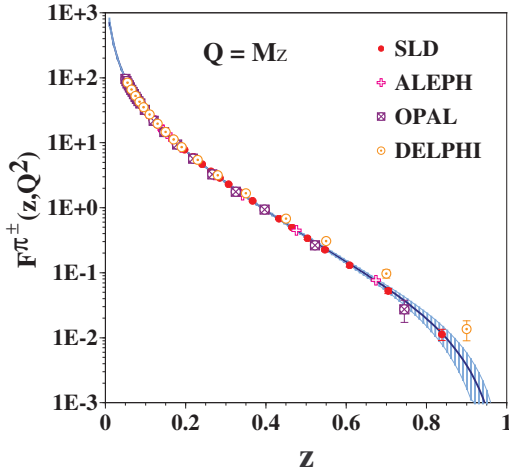


FIG. 2: (Color online) Comparison of our NLO results with pion-production data at $Q = M_Z$ without separation on initial partons by the ALEPH, DELPHI, OPAL, and SLD collaborations.

parametrization; however, some DELPHI data are outside the range of our theoretical estimations. There may be inconsistency among the data sets. However, we did not remove the DELPHI data from the analysis because the obtained functions and the total χ^2 did not change significantly even if they are excluded from the data set. The heavy-quark data also deviate slightly from the theoretical calculations, which result in the relatively large χ^2 contributions.

The kaon fit results are shown in Figs. 5 and 6. The kaon data are reproduced well as shown in these figures. There is no data which indicates significant deviation from the uncertainty regions, which is reflected in the smaller χ^2 ($\chi^2/\text{d.o.f.}=1.34$ in NLO) than the value in the pion analysis ($\chi^2/\text{d.o.f.}=1.73$). However, the bottom-quark data by the SLD are not well explained in the region, $0.4 < z < 0.5$.

The proton results are shown in Figs. 7 and 8. Most of the data are within the uncertainty bands. However, there are serious deviations for the OPAL data, which results in the huge χ^2 value ($\chi^2=110.6$ in NLO) for only ten data points. Since only the OPAL data are different from the other ones by the ALEPH, DELPHI, and SLD collaborations, there is an inconsistency problem for the OPAL measurements.

These figures indicate that our fits are successful. The uncertainty bands become large at small- and large- z regions, so that experimental measurements and theoretical studies are needed to determine the fragmentation functions in the wide- z range.

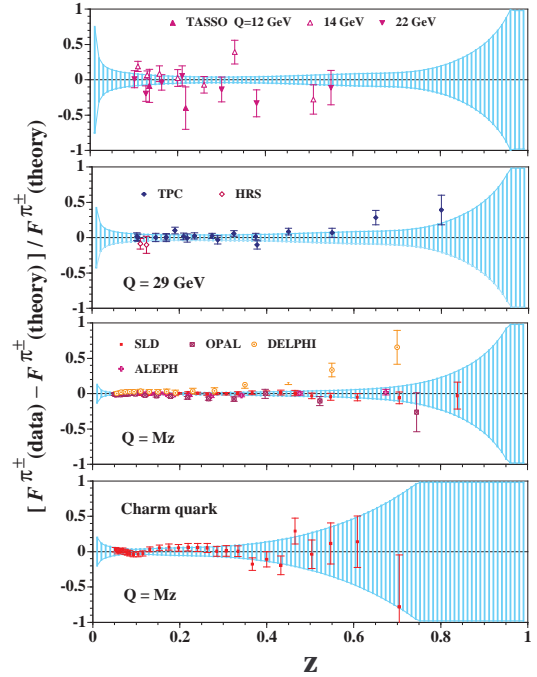


FIG. 3: (Color online) Comparison with charged-pion production data by the TASSO, TPC, HRS, ALEPH, DELPHI, OPAL, and SLD collaborations. The rational differences between the data and theoretical calculations are shown as a function of z . The average scale $Q=16$ GeV is taken for theoretical calculations in the top figure with the TASSO data.

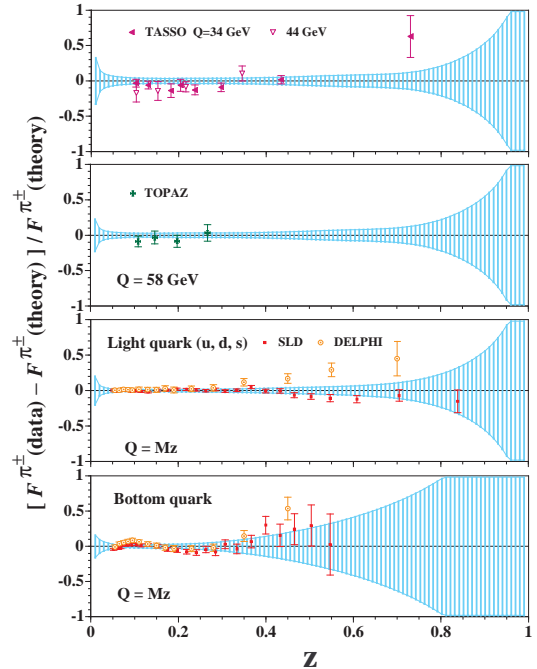


FIG. 4: (Color online) Comparison with charged-pion production data by the TASSO, TOPAZ, DELPHI, and SLD collaborations. The scale is $Q=39$ GeV for theoretical calculations in the top figure.

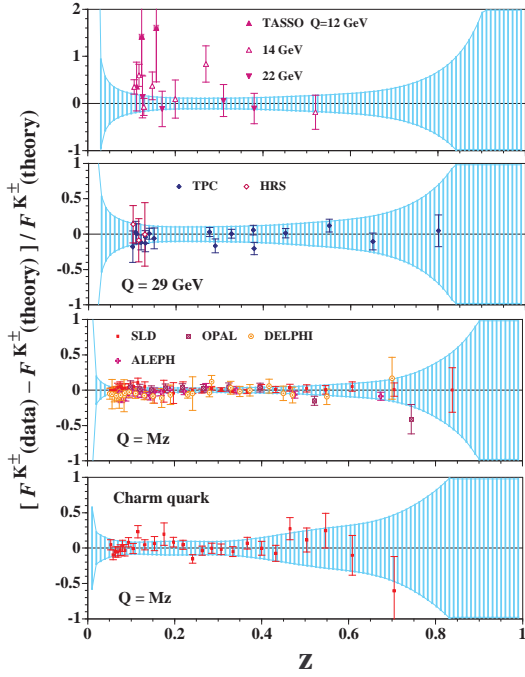


FIG. 5: (Color online) Comparison with charged-kaon production data by the TASSO, TPC, HRS, ALEPH, DELPHI, OPAL, and SLD collaborations. The rational differences between the data and theoretical calculations are shown. The scale is $Q=16$ GeV for theoretical calculations in the top figure.

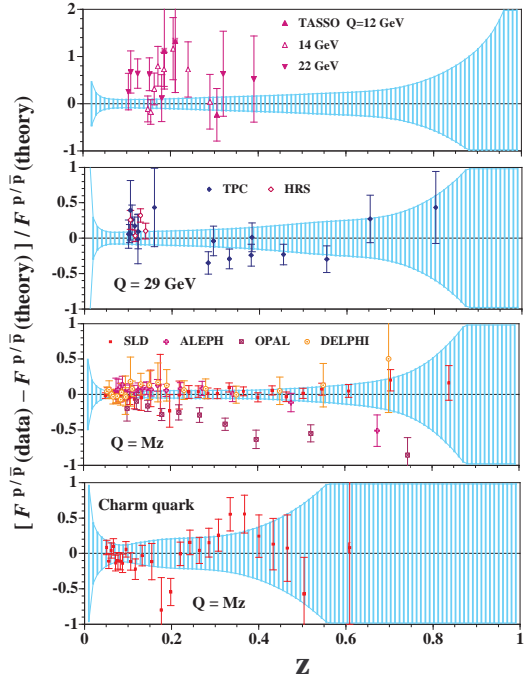


FIG. 7: (Color online) Comparison with proton/anti-proton production data by the TASSO, TPC, HRS, ALEPH, DELPHI, OPAL, and SLD collaborations. The rational differences between the data and theoretical calculations are shown. The scale is $Q=16$ GeV for theoretical calculations in the top figure.

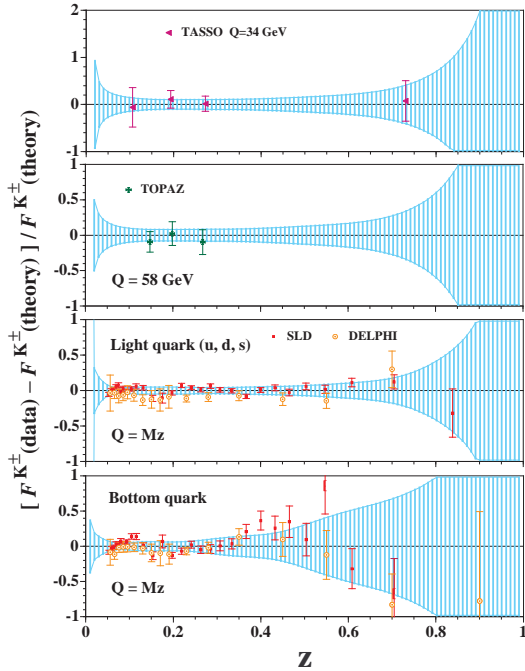


FIG. 6: (Color online) Comparison with charged-kaon production data by the TASSO, TOPAZ, DELPHI, and SLD collaborations. The scale is $Q=34$ GeV for theoretical calculations in the top figure.

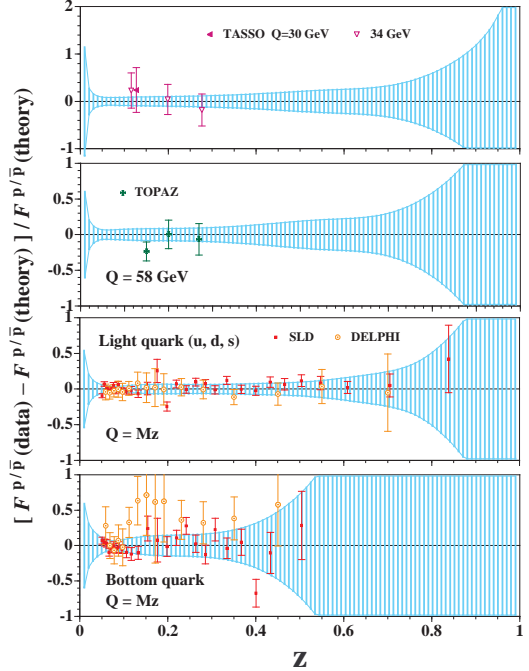


FIG. 8: (Color online) Comparison with proton/anti-proton production data by the TASSO, TOPAZ, DELPHI, and SLD collaborations. The scale is $Q=32$ GeV for theoretical calculations in the top figure.

B. Optimum fragmentation functions and their uncertainties

The obtained fragmentation functions and their uncertainties are shown for π^+ in Figs. 9 and 10. The gluon, up-quark, and anti-up-quark functions are shown at $Q^2=1 \text{ GeV}^2$ in Fig. 9. The charm- and bottom-quark functions are shown at their thresholds. The dashed and solid curves indicate LO and NLO results, and the dark- and light-shaded areas indicate their one- σ uncertainty regions estimated by the Hessian method for the LO and NLO, respectively. There are differences between the LO and NLO functions. The gluon function becomes larger in NLO than the LO one, whereas the quark functions are smaller in NLO. In the NLO, the favored function $D_u^{\pi^+}$ is the largest, and the disfavored one $D_{\bar{u}}^{\pi^+}$ is smaller than $D_u^{\pi^+}$. The gluon function is in-between, and its moment (M_g) is roughly given by their average, $(M_u + M_{\bar{u}})/2$, which agrees with the assumption in Ref. [5].

Since the experimental data are shown by the sum of light-quark flavors, the flavor separation as defined by the favored and disfavored initial functions introduces uncertainties. For example, Fig. 4 indicates 2% error coming directly from the experimental data on the light-quark (u, d, s) fragmentation function at $z = 0.2$ and $Q = M_Z$, whereas the flavor-separated u -quark function in the NLO has 30% error at $z = 0.2$ in Fig. 10. In order to find such a flavor-separation effect on the uncertainties at $Q = 1 \text{ GeV}$, the data should be fitted by the function $D_{q_s}^h = N_{q_s}^h z^{\alpha_{q_s}^h} (1-z)^{\beta_{q_s}^h}$ where $q_s = u + \bar{u} + d + \bar{d} + s + \bar{s}$.

An error from the assumed functional form is not included in estimating the uncertainty bands. We fixed one of the gluon parameters ($\beta_g = 8$), so that the uncertainty could be underestimated in $zD_g^{\pi^+}$ at large z . However, it would not affect the figure of $zD_g^{\pi^+}$ as long as $\beta_g \gg 1$ because the distribution itself is small at large z .

The errors are large in both LO and NLO, which means that the fragmentation functions are not well determined particularly at small Q^2 . However, it is important to find that all the functions for the pion are determined much better in the NLO analysis than the LO ones because the uncertainty bands are smaller in Fig. 9. It is especially noteworthy that the gluon function is determined well in the NLO. The gluonic contributions affect the cross section through the NLO coefficient function and NLO splitting functions. Therefore, the shrinkage of the error band suggests that such gluonic effects are reflected in the current inclusive data for the pion. In particular, the TASSO collaboration provided many data in the small Q^2 region ($Q^2 \ll M_Z^2$), and they are important for identifying such NLO effects in comparison with other data at $Q^2 = M_Z^2$. The reason why the uncertainties are large at small z , especially in the up and charm functions, is since small- z data are not included in the analysis.

The functions for the pion are evolved to $Q^2 = M_Z^2$, and the results are shown in Fig. 10. The functions become steep ones peaked at $z = 0$, and the uncertainties

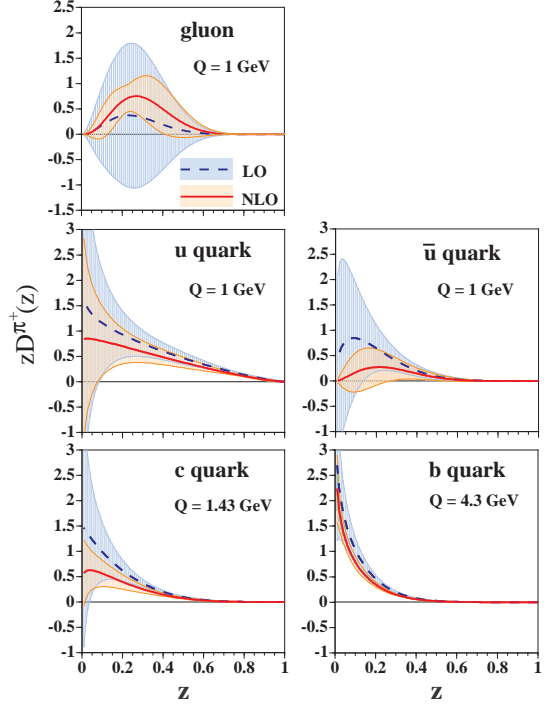


FIG. 9: (Color online) Fragmentation functions and their uncertainties are shown for π^+ at $Q^2=1 \text{ GeV}^2$, m_c^2 , and m_b^2 . The dashed and solid curves indicate LO and NLO results, and the LO and NLO uncertainties are shown by the dark- and light-shaded bands, respectively.

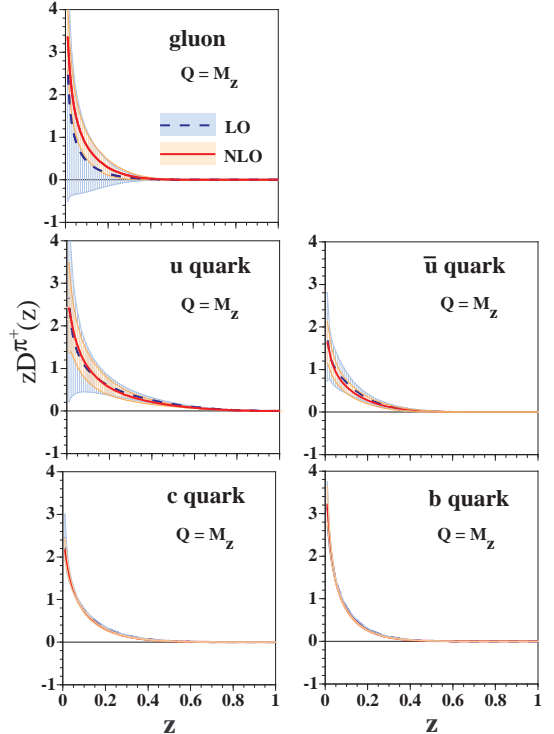


FIG. 10: (Color online) Fragmentation functions and their uncertainties are shown for π^+ at $Q^2 = M_Z^2$. The notations are the same as Fig. 9.

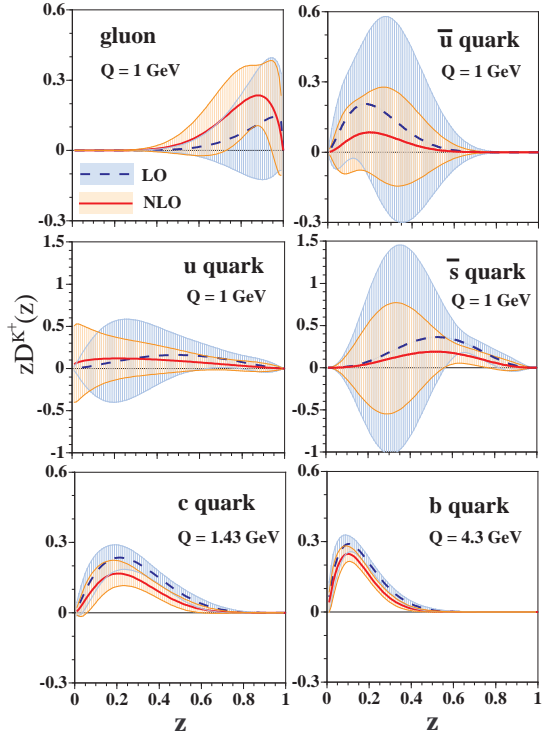


FIG. 11: (Color online) Fragmentation functions and their uncertainties are shown for K^+ at $Q^2=1 \text{ GeV}^2$, m_c^2 , and m_b^2 . The notations are the same as Fig. 9.

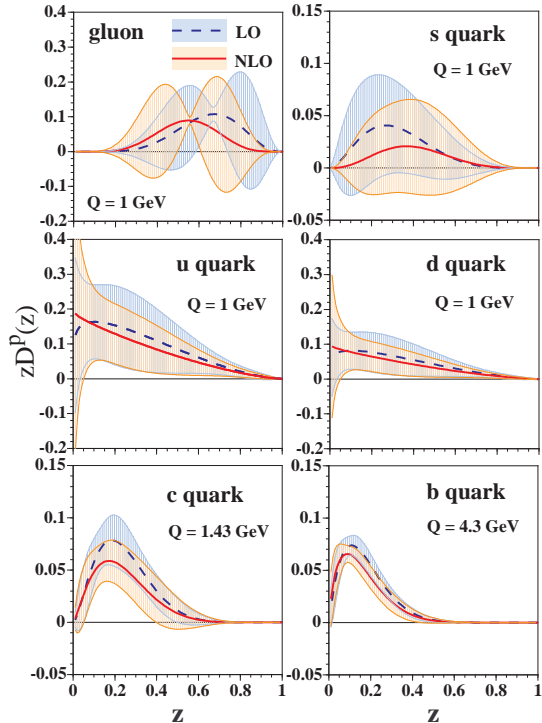


FIG. 12: (Color online) Fragmentation functions and their uncertainties are shown for the proton at $Q^2=1 \text{ GeV}^2$, m_c^2 , and m_b^2 . The notations are the same as Fig. 9.

become relatively small in comparison with the ones in Fig. 9. However, the gluon uncertainties are still large particularly in the LO. The results in Figs. 9 and 10 indicate that the fragmentation functions are not well determined in the small Q^2 region although their uncertainties are relatively small at large Q^2 ($\sim M_Z^2$) especially in the NLO. Therefore, if the fragmentation functions are used in the small Q^2 or small p_T region ($Q^2, p_T^2 \ll M_Z^2$) such as the lepton-scattering processes [1] of COMPASS, HERMES, and JLab (Thomas Jefferson National Accelerator Facility) and the hadron collisions of RHIC [2], it is very important to indicate the uncertainty ranges of the fragmentation functions.

The obtained fragmentation functions and their uncertainties are shown for K^+ in Fig. 11 at $Q^2=1 \text{ GeV}^2$, m_c^2 , and m_b^2 . There are similar tendencies to the pion results. The obtained gluon function in the NLO is larger than the LO one as the pion case, whereas the quark functions are smaller. It is interesting to find that the anti-strange function is generally larger than the up function: $D_{\bar{s}}^{K^+} > D_u^{K^+}$, which could be interpreted in the following way. In order to create K^+ from a parent \bar{s} (or u), a $u\bar{u}$ ($s\bar{s}$) pair needs to be created. Since the strange-quark mass is larger, the $s\bar{s}$ creation could be suppressed in comparison with the $u\bar{u}$ creation, which leads to the inequality. However, the large uncertainty bands indicate that the separation between u and \bar{s} functions is difficult.

There is a conspicuous difference between the gluon functions for the pion and kaon. The gluon function ($zD_g^{K^+}$) is peaked at large z , whereas it is at $z = 0.2 \sim 0.3$ in the pion. Even if an initial distribution with a peak at small z is supplied in the χ^2 fit, the outcome is always peaked at large z . It could be physically understood in the following simple picture. In order to produce K^+ from a gluon, the gluon should first split into a $s\bar{s}$ pair. Then, another gluon is emitted from the s or \bar{s} quark, and it subsequently splits into a $u\bar{u}$ pair. It requires higher energy for the parent gluon to produce the $s\bar{s}$ pair ($g \rightarrow s\bar{s}$) in the kaon creation than the one for a $u\bar{u}$ pair ($g \rightarrow u\bar{u}$) or $d\bar{d}$ pair ($g \rightarrow d\bar{d}$) in the pion creation because of the mass difference. The higher energy means that the function is peaked at larger z in the kaon.

The kaon functions also have large uncertainties in both favored and disfavored cases. They have slightly larger errors than the pionic ones if the ratios $\delta D_i/D_i$ are considered. The uncertainty bands become smaller in NLO than the LO ones. However, the NLO improvement is not as clear as the pionic one. A possible reason is that many accurate data are not taken at small Q^2 ($\ll M_Z^2$), for example, by the TASSO collaboration as for the pion.

The fragmentation functions for the proton are shown in Fig. 12 at $Q^2=1 \text{ GeV}^2$, m_c^2 , and m_b^2 . Here, the gluon moments are fixed by the favored and disfavored moments, so that they are almost the same in LO and NLO. As expected, the favored functions D_u^p and D_d^p are larger than the disfavored functions. The gluon functions have peaks in the medium- z region. In general, the proton

functions are also not determined well, and the uncertainties are as large as the kaonic ones. The NLO improvement is also not obvious in the proton. This fact suggests that the current proton and antiproton data should not be much sensitive to the NLO corrections.

Since the gluon moment is given by the average of favored and disfavored moments, the error of the gluon function D_g^p could be underestimated. A noticeable difference from the pion and kaon figures is that the gluon uncertainty bands shrink in the region $0.5 < z < 0.7$, which is caused by fixing the moment. There are large contributions from the diagonal terms in Eq. (39). The term $(\partial D_g/\partial M_g)^2$ is a smooth function of z with a peak in the same position as the function D_g . On the other hand, $(\partial D_g/\partial \alpha_g)^2$ and $(\partial D_g/\partial \beta_g)^2$ have double peaks, which come from destructive interferences between two derivative terms. For example, the parameter N_g depends on the parameter β_g by Eq. (13). The term $\partial N_g/\partial \beta_g$ is positive, whereas there is a negative contribution from the derivative of $(1-z)^{\beta_g}$. In the pion case, $(\partial D_g/\partial M_g)^2 H_{M_g M_g}^{-1}$ is several times larger than $(\partial D_g/\partial \alpha_g)^2 H_{\alpha_g \alpha_g}^{-1}$, so that such double-peak structure does not appear in the uncertainty band in Fig. 9. However, the term $(\partial D_g/\partial M_g)^2 H_{M_g M_g}^{-1}$ does not exist in the proton analysis since the parameter M_g is fixed. Therefore, the double-peak shape of $(\partial D_g/\partial \beta_g)^2 H_{\beta_g \beta_g}^{-1}$ becomes apparent in Fig. 12.

The determined fragmentation functions and their uncertainties can be calculated by using a library code, which is obtained from our web page [35]. The details are explained on the web page and distributed files.

In these analyses for the pion, kaon, and proton, the charm and bottom functions are determined mainly from the heavy-quark tagging data by the SLD and DELPHI collaborations. The light-quark functions are constrained especially by the accurate data of the SLD. In order to determine the fragmentation functions accurately, we need low-energy data possibly by the Belle and Babar collaborations. The low-energy data should be important for the determination of the gluon functions D_g^h which are essential for describing the low- p_T hadron productions, for example, at RHIC.

The fragmentation functions for π^- , K^- , and \bar{p} can be calculated from the obtained functions by using the relations in Eqs. (34) and (35). The fragmentation functions for π^0 , K^0 , \bar{K}^0 , n , and \bar{n} can be calculated by using the determined functions for the π^+ , K^+ , and proton. The relations are explained in Appendix A.

C. Comparison with other parametrizations

Our NLO fragmentation functions are compared with other parametrizations by KKP [4], AKK [4], and Kretzer [5] in Figs. 13, 14, and 15 for the pion, kaon, and proton/anti-proton, respectively. Since π^+ , K^+ , and proton are not separated from π^- , K^- , and anti-proton in

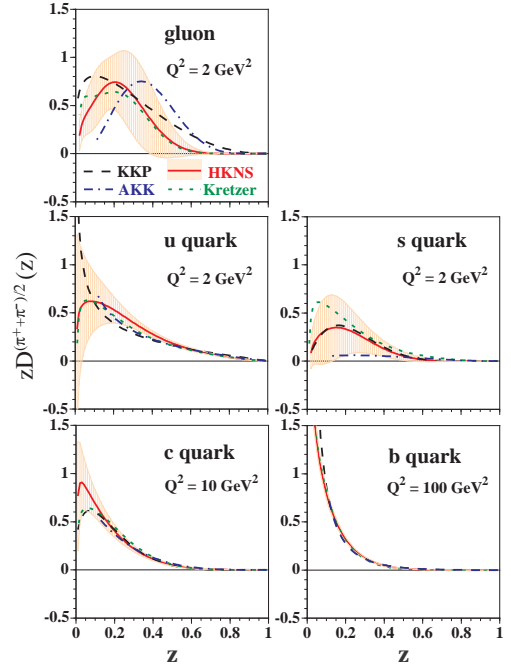


FIG. 13: (Color online) The NLO fragmentation functions for the pion, $z(D_i^{\pi^+} + D_i^{\pi^-})/2$, are compared with other parametrizations at $Q^2=2$ GeV², 10 GeV², and 100 GeV². The solid, dashed, dash-dotted, and dotted curves indicate HKNS, KKP, AKK, and Kretzer parametrizations, respectively, in the NLO $\overline{\text{MS}}$ scheme. The HKNS uncertainty bands are shown by the shaded areas.

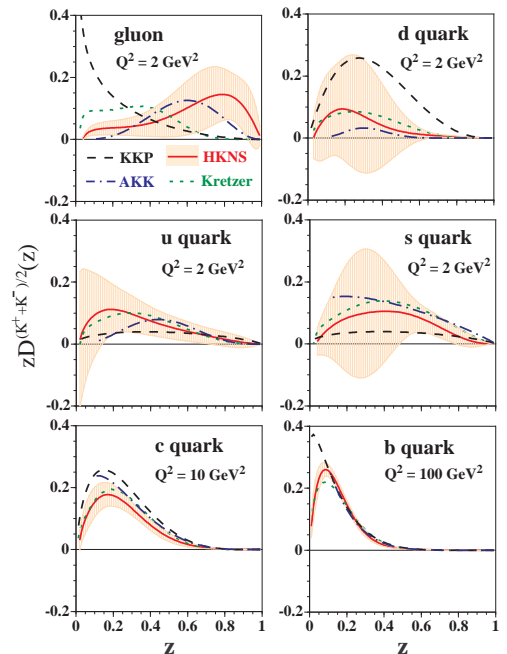


FIG. 14: (Color online) The NLO fragmentation functions for the kaon, $z(D_i^{K^+} + D_i^{K^-})/2$, are compared with other parametrizations at $Q^2=2$ GeV², 10 GeV², and 100 GeV². The notations are the same as Fig. 13.

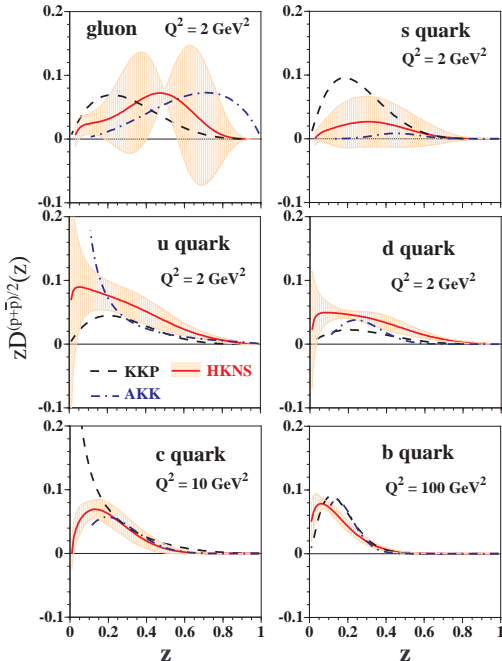


FIG. 15: (Color online) The NLO fragmentation functions for the proton/anti-proton, $z(D_i^p + D_i^{\bar{p}})/2$, are compared with other parametrizations at $Q^2=2$ GeV², 10 GeV², and 100 GeV². The notations are the same as Fig. 13.

the KKP and AKK parametrizations, the combinations $z(D_i^{\pi^+} + D_i^{\pi^-})/2$, $z(D_i^{K^+} + D_i^{K^-})/2$, and $z(D_i^p + D_i^{\bar{p}})/2$ are shown. Our parametrization is denoted HKNS (Hirai, Kumano, Nagai, Sudoh) in these figures. The light-quark functions are separated in the AKK parametrization due to additional OPAL data, which are not used in the other analyses. The KKP, AKK, and Kretzer distributions are calculated by using their library codes. The small- z part is not plotted for the AKK because their code does not support the region, $z < 0.1045$ by considering resummation effects in comparison with the data. The heavy-quark thresholds are taken $4m_c^2$ and $4m_b^2$ for the fragmentation functions in the KKP and AKK parametrizations, whereas they are m_c^2 and m_b^2 in the Kretzer and HKNS analyses. The minimum value of Q^2 in the KKP and AKK codes is $Q^2=2$ GeV². Therefore, comparisons are made at $Q^2=2, 10, \text{ and } 100$ GeV².

If the distributions are compared with each other in Fig. 13 for the pion, they agree well in up-, charm-, and bottom-quark functions. The up-quark function of the KKP has a singular behavior as $z \rightarrow 0$, which is different from the Kretzer's, AKK, and HKNS functions. However, the small- z data are not included in these analyses, so that the differences should not be taken seriously at small z . Since new SLD data in 2004 are accurate and they are not used in other parametrizations, the fragmentation functions could be better determined in our parametrization. The four types of functions are very different in the gluon and disfavored strange-quark functions in Fig. 13. All the gluon functions have various peak positions in the region $0.1 < z < 0.4$ and func-

tional forms are different. Our gluon function roughly agrees with the Kretzer's function. The four strange-quark functions are also much different. Although our strange-quark function is almost equal to the KKP, the Kretzer's (AKK) function is much larger (smaller). However, it is important to find that the gluon and strange-quark functions, needless to say the up-, charm-, and bottom-quark functions, by the KKP, AKK, Kretzer, and HKNS are consistent with each other because they are within the uncertainty bands. This fact indicates that all the analyses are successful and consistent.

For the kaon, the KKP, AKK, Kretzer's, and HKNS results agree well in the charm- and bottom-quark functions as shown in Fig. 14. However, they differ much in the gluon and light-quark functions. In particular, the HKNS and AKK gluon functions are peaked at large z , whereas the KKP diverges at small z and the Kretzer's function is peaked at $z \sim 0.4$. The KKP and Kretzer functions are outside the uncertainty band at small z . Since the parameter α_g is fixed and because of the functional form with the peak at large z , the uncertainty could be underestimated in the small- z region. The large variations among the parametrizations of $D_g^{(K^+ + K^-)}/2$ indicate that the current kaon data are not accurate enough to fix the gluon fragmentation function for the kaon from the scaling violation. Lower-energy data, for example from Belle and BaBar, should be able to improve the situation. The light-quark (u, d, s) functions are also very different; however, they are roughly within the uncertainty band. Except for the gluon function, all the analysis results are consistent in the kaon.

The results agree well with each other in the charm- and bottom-quark functions for the proton and anti-proton as shown in Fig. 15, although there are some differences at small z where experimental data are not used in the analyses. The Kretzer's parametrization is not available for the proton. The three gluon functions are very different but they are roughly within the uncertainty band. It is almost impossible to determine the accurate gluon function at this stage. The disfavored strange-quark functions are also very different. In particular, the KKP (AKK) function is much larger (smaller) than our result. Our favored functions, up- and down-quark ones, are larger than the KKP and AKK functions. However, all these fragmentation functions including the disfavored ones are roughly within the estimated uncertainties.

From these comparisons, we found that the analyses of KKP, AKK, Kretzer, and HKNS are consistent because they are generally within the uncertainty bands estimated by the Hessian method. However, there are noticeable differences in the gluon and light-quark fragmentation functions. They should be clarified by future measurements especially at small Q^2 . The large uncertainties could cause serious effects in discussing hadron-production processes at small p_T such as RHIC, HERMES, and JLab.

V. SUMMARY

Unpolarized fragmentation functions for the pion, kaon, and proton have been determined in the LO and NLO from global analyses of $e^+e^- \rightarrow h+X$ data. Their uncertainties were estimated by the Hessian method. We found the large uncertainties in the fragmentation functions at small Q^2 ($\sim 1 \text{ GeV}^2$) although they become relatively smaller at high energies ($Q^2 \sim M_Z^2$). In particular, the gluon and light-quark fragmentation functions have large uncertainties. However, they are determined more accurately in the NLO analyses than the LO ones for the pion and kaon. Because of the large uncertainties at small Q^2 , it is important that such errors need to be taken into account in analyzing the hadron-production data in high-energy lepton-proton, proton-proton, and nuclear reactions. Low-energy e^+e^- measurements should be valuable for determining especially the gluon fragmentation functions by the scaling violation. A code for calculating the determined fragmentation functions can be obtained from our web page [35].

Acknowledgments

S.K. and M.H. were supported by the Grant-in-Aid for Scientific Research from the Japanese Ministry of Education, Culture, Sports, Science, and Technology. T.-H.N. was supported by the JSPS Research Fellowships for Young Scientists. S.K., T.-H.N., and K.S. thank Institute for Nuclear Theory at the University of Washington for its hospitality and the US Department of Energy for partial support.

APPENDIX A: FRAGMENTATION FUNCTIONS FOR π^0 , K^0 , \bar{K}^0 , n , AND \bar{n}

The fragmentation functions of π^+ , π^- , K^+ , K^- , p , and \bar{p} are extracted from the experiment by assuming charge symmetry in relating $D_i^{\pi^+}$, $D_i^{K^+}$, and D_i^p to the corresponding ones $D_i^{\pi^-}$, $D_i^{K^-}$, and $D_i^{\bar{p}}$ by Eqs. (34) and (35). One may need the fragmentation functions for π^0 , K^0 , \bar{K}^0 , n , or \bar{n} in one's studies of high-energy hadron reactions. The quark compositions of these hadrons are

$\pi^0((u\bar{u}-d\bar{d})/\sqrt{2})$, $K^0(d\bar{s})$, $\bar{K}^0(\bar{d}s)$, $n(udd)$, and $\bar{n}(\bar{u}\bar{d}\bar{d})$. Considering these compositions, we relate the obtained functions to the ones for π^0 , K^0 , \bar{K}^0 , n , and \bar{n} [4]. The π^0 functions are given by the averages of π^+ and π^- :

$$D_i^{\pi^0}(z, Q^2) = \frac{1}{2}[D_i^{\pi^+}(z, Q^2) + D_i^{\pi^-}(z, Q^2)]. \quad (\text{A1})$$

The K^0 functions are also calculated by the relations:

$$\begin{aligned} D_d^{K^0}(z, Q^2) &= D_u^{K^+}(z, Q^2), \\ D_s^{K^0}(z, Q^2) &= D_s^{K^+}(z, Q^2), \\ D_u^{K^0}(z, Q_0^2) &= D_u^{K^+}(z, Q_0^2) = D_{\bar{u}}^{K^0}(z, Q_0^2) \\ &= D_d^{K^0}(z, Q_0^2) = D_s^{K^0}(z, Q_0^2), \\ D_{c,b}^{K^0}(z, Q^2) &= D_{c,b}^{K^+}(z, Q^2) = D_{\bar{c},\bar{b}}^{K^0}(z, Q^2), \\ D_g^{K^0}(z, Q^2) &= D_g^{K^+}(z, Q^2). \end{aligned} \quad (\text{A2})$$

However, one should be careful about the following relations at different Q^2 from Q_0^2 because of the NLO evolution:

$$D_{\bar{u}}^{K^0}(z, Q^2) \neq D_d^{K^0}(z, Q^2) \neq D_s^{K^0}(z, Q^2), \quad (\text{A3})$$

although $D_u^{K^0}(z, Q^2) = D_{\bar{u}}^{K^0}(z, Q^2)$ is still valid. Then, \bar{K}^0 functions are related to the K^0 ones by

$$\begin{aligned} D_q^{\bar{K}^0}(z, Q^2) &= D_q^{K^0}(z, Q^2), \\ D_g^{\bar{K}^0}(z, Q^2) &= D_g^{K^0}(z, Q^2). \end{aligned} \quad (\text{A4})$$

The neutron functions are related to the proton ones by

$$\begin{aligned} D_u^n(z, Q^2) &= D_d^p(z, Q^2), \\ D_d^n(z, Q^2) &= D_u^p(z, Q^2), \\ D_i^n(z, Q^2) &= D_i^p(z, Q^2) \quad \text{for } i \neq u, d. \end{aligned} \quad (\text{A5})$$

The anti-neutron functions are then given by

$$\begin{aligned} D_q^{\bar{n}}(z, Q^2) &= D_q^n(z, Q^2), \\ D_g^{\bar{n}}(z, Q^2) &= D_g^n(z, Q^2). \end{aligned} \quad (\text{A6})$$

Using the code in Ref. [35], one should be able calculate the fragmentation functions for π^+ , π^0 , π^- , K^+ , K^- , K^0 , \bar{K}^0 , p , \bar{p} , n , and \bar{n} at given z and Q^2 .

-
- [1] A. Airapetian *et al.* (HERMES Collaboration), Phys. Rev. **D71**, 012003 (2005); S. Kretzer, E. Leader, and E. Christova, Eur. Phys. J. **C22**, 269 (2001); X. Zheng *et al.*, JLab proposal PR04-114 (2004).
[2] S. S. Adler *et al.* (PHENIX collaboration), Phys. Rev. Lett. **91**, 241803 (2003); **93**, 202002 (2004); M. Hirai and K. Sudoh, Phys. Rev. **D71**, 014022 (2005).
[3] <http://www.pv.infn.it/~radici/FFdatabase/>
[4] B. A. Kniehl, G. Kramer, and B. Pötter, Nucl. Phys.

- B582**, 514 (2000) & **B597**, 337 (2001). There are also previous and recent analyses in J. Binnewies, B. A. Kniehl, and G. Kramer, Z. Phys. **C65**, 471 (1995); Phys. Rev. **D52**, 4947 (1995); **D53**, 3573 (1996); S. Albino, B.A. Kniehl, and G. Kramer, Nucl. Phys. **B725**, 181 (2005); **B734**, 50 (2006); B. A. Kniehl and G. Kramer, Phys. Rev. **D71**, 094013 (2005); **D74**, 037502 (2006).
[5] S. Kretzer, Phys. Rev. **D62**, 054001 (2000).
[6] J. Pumplin *et al.*, Phys. Rev. **D65**, 014013 (2001); JHEP

- 0207**, 012 (2002); A. D. Martin, R. G. Roberts, W. J. Stirling, and R. S. Thorne, *Eur. Phys. J.* **C28**, 455 (2003); **C35** (2004) 325.
- [7] J. Blümlein and H. Böttcher, *Nucl. Phys.* **B636**, 225 (2002); M. Hirai, S. Kumano, and N. Saito, *Phys. Rev.* **D69**, 054021 (2004); **D74**, 014015 (2006); E. Leader, A. V. Sidorov, and D. B. Stamenov, *Phys. Rev.* **D73**, 034023 (2006); D. de Florian, G. A. Navarro, and R. Sassot, *Phys. Rev.* **D71**, 094018 (2005).
- [8] M. Hirai, S. Kumano, and T.-H. Nagai, *Phys. Rev.* **C70**, 044905 (2004); research in progress.
- [9] F. Halzen and A. D. Martin, *Quarks and Leptons: An Introductory Course in Modern Particle Physics*, John Wiley & Sons (1984).
- [10] R. K. Ellis, W. J. Stirling, and B. R. Webber, *QCD and Collider Physics*, Cambridge University Press (1996).
- [11] P. Nason and B. R. Webber, *Nucl. Phys.* **B421**, 473 (1994); Erratum, *ibid.* **B480**, 755 (1996). See also G. Altarelli, R. K. Ellis, G. Martinelli, and S. Y. Pi, *Nucl. Phys.* **B160**, 301 (1979); W. Furmanski and R. Petronzio, *Z. Phys.* **C11**, 293 (1982). NNLO results are in A. Mitov and S. Moch, *Nucl. Phys.* **B751** (2006) 18.
- [12] M. Stratmann and W. Vogelsang, *Nucl. Phys.* **B496** (1997) 41. NNLO results are in A. Mitov, S. Moch, and A. Vogt, *Phys. Lett.* **B638** (2006) 61.
- [13] M. Miyama and S. Kumano, *Comput. Phys. Commun.* **94**, 185 (1996); M. Hirai, S. Kumano, and M. Miyama, *Comput. Phys. Commun.* **108**, 38 (1998); **111**, 150 (1998); S. Kumano and T.-H. Nagai, *J. Comput. Phys.* **201**, 651 (2004).
- [14] S. Kumano, *Phys. Rep.* **303**, 183 (1998); G. T. Garvey and J.-C. Peng, *Prog. Part. Nucl. Phys.* **47**, 203 (2001).
- [15] R. Jakob, P. J. Mulders, and J. Rodrigues, *Nucl. Phys.* **A626**, 937 (1997).
- [16] R. Brandelik *et al.* (TASSO collaboration), *Phys. Lett.* **B94**, 444 (1980).
- [17] M. Althoff *et al.* (TASSO collaboration), *Z. Phys.* **C17**, 5 (1983).
- [18] W. Braunschweig *et al.* (TASSO collaboration), *Z. Phys.* **C42**, 189 (1989).
- [19] H. Aihara *et al.* (TPC collaboration), *Phys. Rev. Lett.* **52**, 577 (1984); **61**, 1263 (1988).
- [20] M. Derrick *et al.* (HRS collaboration), *Phys. Rev.* **D35**, 2639 (1987).
- [21] R. Itoh *et al.* (TOPAZ collaboration), *Phys. Lett.* **B345**, 335 (1995).
- [22] K. Abe *et al.* (SLD collaboration), *Phys. Rev.* **D69**, 072003 (2004).
- [23] D. Buskulic *et al.* (ALEPH collaboration), *Z. Phys.* **C66**, 355 (1995); R. Barate *et al.*, *Phys. Rep.* **294**, 1 (1998).
- [24] R. Akers *et al.* (OPAL collaboration), *Z. Phys.* **C63**, 181 (1994).
- [25] P. Abreu *et al.* (DELPHI collaboration), *Eur. Phys. J.* **C5**, 585 (1998).
- [26] P. Abreu *et al.* (DELPHI collaboration), *Nucl. Phys.* **B444**, 3 (1995).
- [27] H. Schellman *et al.* (MARK-II collaboration), *Phys. Rev.* **D31**, 3013 (1985).
- [28] W. Bartel *et al.* (JADE collaboration), *Phys. Lett.* **B104**, 325 (1981).
- [29] <http://durpdg.dur.ac.uk/hepdata/online/ee/eeindex.html>.
- [30] S. Albino, B.A. Kniehl, G. Kramer, and W. Ochs, *Phys. Rev.* **D73**, 054020 (2006).
- [31] There is a parametrization without separating produced hadrons: L. Bourhis, M. Fontannaz, J. P. Guillet, and M. Werlen, *Eur. Phys. J.* **C19**, 89 (2001).
- [32] A. D. Martin, R. G. Roberts, W. J. Stirling, and R. S. Thorne, *Eur. Phys. J.* **C23**, 73 (2002); *Phys. Lett.* **B531**, 216 (2002).
- [33] F. James, CERN Program Library Long Writeup D506. See <http://wwwasdoc.web.cern.ch/wwwasdoc/minuit/minmain.html>.
- [34] For example, see <http://wwwasdoc.web.cern.ch/wwwasdoc/minuit/node33.html>, <http://www.nrbook.com/b/bookfpdf/fl5-6.pdf>, <http://ccwww.kek.jp/pdg/2006/reviews/statrpp.pdf>.
- [35] A code for calculating the obtained fragmentation functions is available at <http://research.kek.jp/people/kumanos/ffs.html>.